AJNR

A Diagnostic Algorithm for Posterior Fossa Tumors in Children: A Validation Study

C.A.P.F. Alves, U. Löbel, J.S. Martin-Saavedra, S. Toescu, M.H. Tsunemi, S.R. Teixeira, K. Mankad, D. Hargrave, T.S. Jacques, C. da Costa Leite, F.G. Gonçalves, A. Vossough and F. D'Arco

A Diagnostic Algorithm for Posterior Fossa Tumors in Children: A Validation Study

C.A.P.F. Alves, U. Löbel, J.S. Martin-Saavedra, S. Toescu, M.H. Tsunemi, S.R. Teixeira, K. Mankad, D. Hargrave, T.S. Jacques, C. da Costa Leite, F.G. Gonçalves, A. Vossough, and F. D'Arco

ABSTRACT

BACKGROUND AND PURPOSE: Primary posterior fossa tumors comprise a large group of neoplasias with variable aggressiveness and short and long-term outcomes. This study aimed to validate the clinical usefulness of a radiologic decision flow chart based on previously published neuroradiologic knowledge for the diagnosis of posterior fossa tumors in children.

MATERIALS AND METHODS: A retrospective study was conducted (from January 2013 to October 2019) at 2 pediatric referral centers, Children's Hospital of Philadelphia, United States, and Great Ormond Street Hospital, United Kingdom. Inclusion criteria were younger than 18 years of age and histologically and molecularly confirmed posterior fossa tumors. Subjects with no available preoperative MR imaging and tumors located primarily in the brain stem were excluded. Imaging characteristics of the tumors were evaluated following a predesigned, step-by-step flow chart. Agreement between readers was tested with the Cohen κ, and each diagnosis was analyzed for accuracy.

RESULTS: A total of 148 cases were included, with a median age of 3.4 years (interquartile range, 2.1–6.1 years), and a male/female ratio of 1.24. The predesigned flow chart facilitated identification of pilocytic astrocytoma, ependymoma, and medulloblastoma *sonic hedgehog* tumors with high sensitivity and specificity. On the basis of the results, the flow chart was adjusted so that it would also be able to better discriminate atypical teratoid/rhabdoid tumors and medulloblastoma groups 3 or 4 (sensitivity = 75%–79%; specificity = 92%–99%). Moreover, our adjusted flow chart was useful in ruling out ependymoma, pilocytic astrocytomas, and medulloblastoma *sonic hedgehog* tumors.

CONCLUSIONS: The modified flow chart offers a structured tool to aid in the adjunct diagnosis of pediatric posterior fossa tumors. Our results also establish a useful starting point for prospective clinical studies and for the development of automated algorithms, which may provide precise and adequate diagnostic tools for these tumors in clinical practice.

ABBREVIATIONS: AT/RT = atypical teratoid/rhabdoid tumor; LR = likelihood ratio; NPV = negative predictive value; PA = pilocytic astrocytoma; PPV = positive predictive value; WNT = wingless; SHH = sonic hedgehog

In the past 10 years, there has been an exponential increase in knowledge of the molecular characteristics of pediatric brain tumors, which was only partially incorporated in the 2016 World Health Organization Classification of Tumors of the Central Nervous System.[1] The main update in the 2016

Classification was the introduction of the molecular profile of a tumor as an important factor for predicting different biologic behaviors of entities which, on histology, look very similar or even indistinguishable.[2] A typical example is the 4 main groups of medulloblastoma: *wingless* (*WNT*), *sonic hedgehog* (*SHH*) with or without the p53 mutation, group 3, and group 4. Although they may appear similar on microscopy, these categories have distinct molecular profiles, epidemiology, prognosis, and embryologic origin.[3]

Subsequent to the publication of the 2016 World Health Organization Classification, further studies have identified even more molecular subgroups of medulloblastoma with possible prognostic implications[4] and also at least 3 new molecular subgroups of atypical teratoid/rhabdoid tumor (AT/RT)[5] and several subgroups of ependymoma.[6] MR imaging shows promise as a technique for differentiating histologic tumors and their molecular subgroups. This capability relies on not only various imaging characteristics but also the location and spatial extension of the
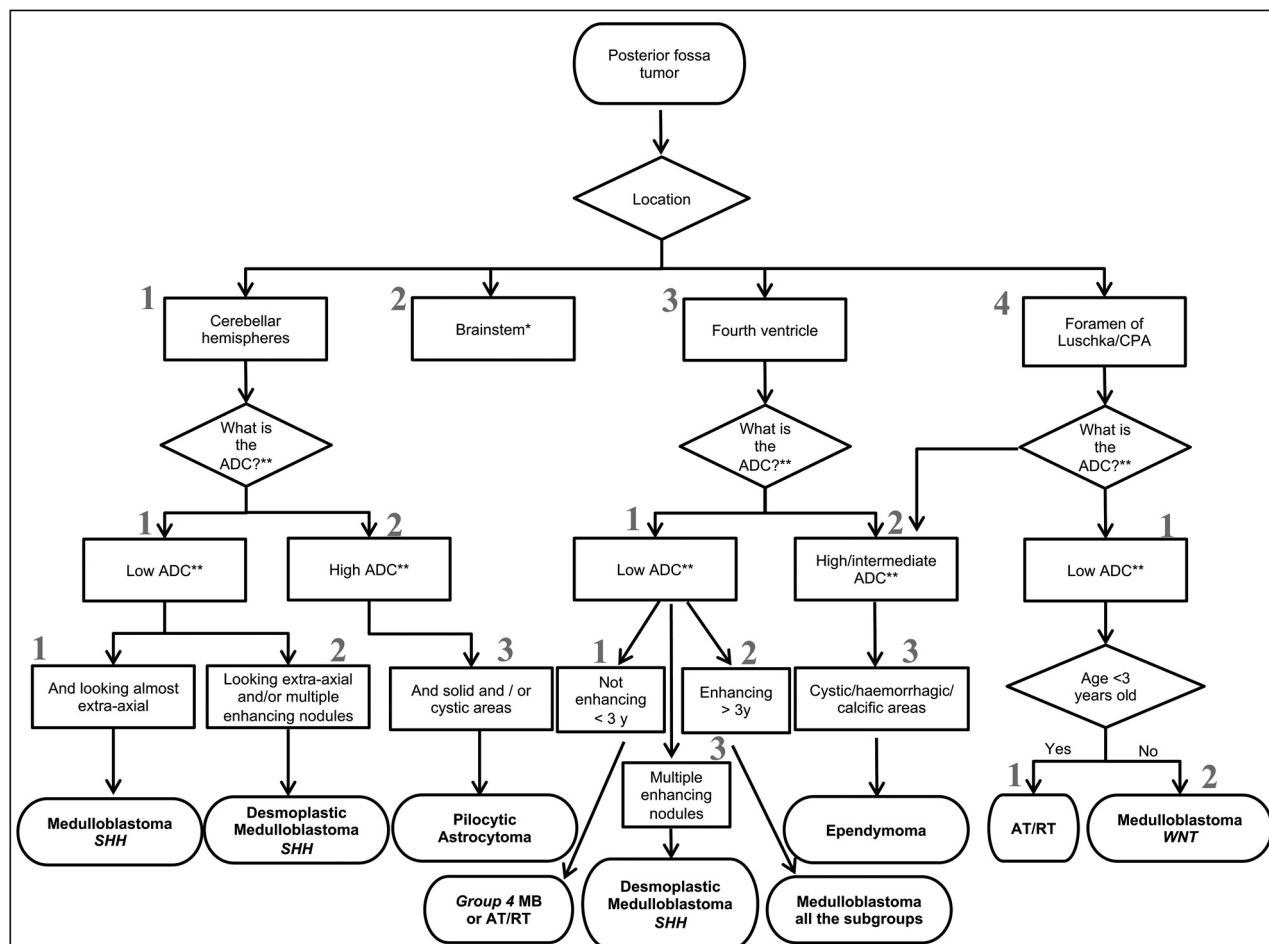
FIG 1. Predesigned radiologic flow chart created according to the literature before diagnostic accuracy analysis. The *asterisk* indicates brain stem tumors excluded from the analysis. *Double asterisks* indicate relative to gray matter. Modified with permission from D'Arco et al.[11]

tumor, evident on MR imaging, which can be traced to the embryologic origin of the neoplastic cells.[5,7-10]

One approach to the challenge of identifying imaging characteristics of different tumors in children is to use artificial intelligence. Yet despite this exciting innovation, correctly identifying the location of the mass and its possible use as an element for differential diagnosis still requires the expertise of an experienced radiologist. Previously, D'Arco et al[11] proposed a flow chart (Fig 1) for the differential diagnosis of posterior fossa tumors in children based on epidemiologic, imaging signal, and location characteristics of the neoplasm. The aims of the current study were the following: 1) to validate, in a retrospective, large cohort of posterior fossa tumors from 2 separate pediatric tertiary centers, the diagnostic accuracy of that flow chart, which visually represents the neuroadiologist's mental process in making a diagnosis of posterior fossa tumors in children, 2) to describe particular types of posterior fossa lesions that are not correctly diagnosed by the initial flow chart, and 3) to provide an improved, clinically accessible flow chart based on the results.

MATERIALS AND METHODS

Setting and Subjects
A retrospective, cross-sectional study from 2 large tertiary referral pediatric hospitals in 2 countries (Children's Hospital of Philadelphia,

United States, and Great Ormond Street Hospital, London, United Kingdom) was performed on the basis of patient records spanning January 2013 to October 2019 in accordance with the Strengthening the Reporting of Observational Studies in Epidemiology (STROBE) statement.[12] This study was conducted under 2 research protocols (IRB No. 18–015588 and CA Reg No. 2504), approved by the respective institutional review boards at each center.

Subjects were identified by electronic search of brain MR imaging reports and the electronic health record systems. The following terms/diagnoses were used for the search: "brain tumor," "posterior fossa tumor," "brain neoplasia," "posterior fossa neoplasia," "cerebellar tumor," "cerebellar neoplasia," "medulloblastoma," "AT/RT," "atypical teratoid/rhabdoid tumor," "ependymoma," "pilocytic astrocytoma." Results were screened, and subjects younger than 18 years of age with a histologically and genetically confirmed diagnosis of posterior fossa tumor, according to the 2016 World Health Organization classification, were selected.[2] Subjects with no available preoperative MR imaging study, those with low-quality MR imaging studies, and those without diffusion imaging on their MR imaging study were excluded. Subjects with tumors located primarily in the brain stem were also excluded.

Variables
Age at first MR imaging (before histologic/pathologic confirmation of the tumor), sex, and histologic and genetic/molecular results

were obtained from the electronic medical records. Two experienced pediatric neuroradiologists independently reviewed these initial MR imaging studies at each institution (C.A.P.F.A., A.V., F.D., and U.L.), blinded to the final diagnosis. Imaging characteristics were evaluated following a step-by-step numeric flow chart, with a digit assigned to each level and subsequent branch, providing a flow chart and a 3-digit numeric sequence code for each diagnosis end point to be used in the analysis (Fig 1). The flow chart took into account the following: 1) tumor location, 2) ADC map signal intensity in comparison with gray matter, 3) internal architecture, 4) contrast enhancement, and 5) the patient's age. The flow chart was designed before the initiation of the study; it was based on a review on the topic by D'Arco et al.[11] Before starting the blinded analysis of the cohort, one of the readers (C.A.P.F.A.) performed a pilot evaluation using the first 8 cases from each institution (16/148; 10.8%) to confirm the applicability of the flow chart multiple weeks before the formal evaluation.

Statistical Analysis
Visual inspection of the histogram showed non-normal distribution, which was confirmed with the Shapiro-Wilk test ($P < .001$) for all numeric variables. Categoric variables are described with percentage and frequency, and numeric variables, with median and interquartile range. Statistical analysis was performed using R statistical and computing software, Version 3.5.3 for Windows (http://www.r-project.org/).

Diagnostic accuracy of the flow chart was verified through a 2 × 2 contingency table and calculation of sensitivity, specificity, positive predictive values (PPV), and negative predictive value (NPV). To estimate accuracy and effect size, we estimated 95% CIs for sensitivity, specificity, PPV, and NPV. The diagnostic accuracy analysis was performed for each diagnosis, with molecular/histologic diagnosis as the criterion standard comparison. Because flow chart numeric sequences 312 and 311 of the predesigned flow chart would not provide a single unique final tumor molecular diagnosis, we later adjusted the sequences according to the most prevalent diagnosis. The modified flow chart reflects these adjustments. Last, we recalculated diagnostic accuracy tests on the basis of the adjustments for these 2 flow chart modifications. The clinical applicability of findings was further explored with positive and negative likelihood ratios (LR+ and LR–, respectively), and on the basis of changes in probability from the LR described by McGee.[13] Clinical applicability to rule in diagnosis was considered if the 95% CI of LR+ was above 10. Clinical applicability to rule out diagnosis was considered if the 95% CI of LR– was below 0.5.

RESULTS
Histologic Diagnosis and Demographics
One hundred forty-eight subjects were included. The median age at MR imaging was 3.4 years, (interquartile range = 2.1–6.1 years), and the male/female ratio was 1.24. Fifty-four (36.5%) patients had a histologic diagnosis of medulloblastoma, 56 (37.5%) had pilocytic astrocytoma (PA), 12 (8.1%) had AT/RT, and 19 (12.8%) had ependymoma. Medulloblastomas were also subclassified according to molecular subtypes including 14/54 (26%) SHH; 7/54 (13%) WNT; 5/54 (9%) group 3; 9/54 (17%) group 4; and 19/54 (35%) group 3 or 4 (separation of groups 3 and 4 was not always

easily possible). Seven cases (5%) had a diagnosis of other tumors not covered by the flow chart (2 low-grade diffuse astrocytomas not otherwise specified, 1 hemangioblastoma, 2 gangliogliomas, 1 case of Langerhans cell histiocytosis, and 1 meningioma). Agreement between readers at each institution was very high ($\kappa = 0.96$ for both institutions, $P < .001$). Because both institutions had almost perfect agreement, we did a pooled analysis without differentiating per institution. The same diagnosis using the predesigned flow chart was reached for 86% of the cohort. In the 14% of cases in which the same diagnosis was not reached by the 2 readers, disagreement was solved through consensus between the readers.

Diagnosis Using the Flowchart
By means of the predesigned flow chart (Fig 1), the most common diagnosis was PA (numeric sequence 123) ($n = 53$, 36%), followed by medulloblastoma all subgroups (numeric sequence 312) ($n = 35$, 24%), ependymoma (numeric sequence 323) ($n = 17$, 11%), medulloblastoma SHH (numeric sequence 111) ($n = 10$, 7%), medulloblastoma group 4 or AT/RT (numeric sequence 311) ($n = 5$, 3%), AT/RT (numeric sequence 411) ($n = 7$, 5%), ependymoma (numeric sequence 423) ($n = 7$, 5%), desmoplastic medulloblastoma SHH (numeric sequence 112) ($n = 6$, 4%), desmoplastic medulloblastoma SHH (numeric sequence 313) ($n = 3$, 2%), and medulloblastoma WNT (numeric sequence 412) ($n = 5$, 3%). Figure 2 and Table 1 show the statistical results of the sensitivity, specificity, PPV, and NPV of the flow chart per diagnosis.

In cases that followed sequence 311 (medulloblastoma group 4 or AT/RT), 3/5 (60%) were AT/RT, 1/5 (20%) was an ependymoma, and 1/5 (20%) was a medulloblastoma group 4. This finding suggested that sequence 311 catches more tumors in the AT/RT category than in medulloblastoma group 4, so we recalculated the diagnostic accuracy tests considering both 311 and 411 as AT/RTs. As can be appreciated in Fig 2 and Table 1, diagnostic accuracy for cases of AT/RT improved when combining sequences 311 and 411. Of the 35 cases under sequence 312 (medulloblastoma all subgroups), 26/35 (74%) were confirmed as group 3 or 4 (3 confirmed as group 3, eight confirmed as group 4, and 15, as group 3 or 4). The remaining cases under sequence 312 were 3/35 (9%) SHH, 5/35 (14%) WNT, and 1/35 (3%) AT/RT. Figure 3 shows the diagnostic accuracy of sequence 312 to identify medulloblastoma SHH, WNT, and group 3 or 4. For this sequence, the NPV and specificity were higher than the PPV and sensitivity for all other sequences. Table 2 shows the LR analysis per diagnosis and the recommended sequences for the diagnosis. After our analysis and on the basis of Table 1 results, we modified the predesigned flow chart with more precise categorization of the types of tumor. We recommend this new flow chart (Fig 4) for the diagnosis of posterior fossa tumors in children.

Some examples of differentiating posterior fossa tumors from our cohort, diagnosed on the basis of the new flow chart here presented, can be seen in Figs 5 and 6.

DISCUSSION
The 2016 introduction of the new classification of brain tumors based on histologic and molecular characteristics dramatically changed the management of pediatric brain tumors.[1,2,14,15] Tumors with similar histologic appearance being related to
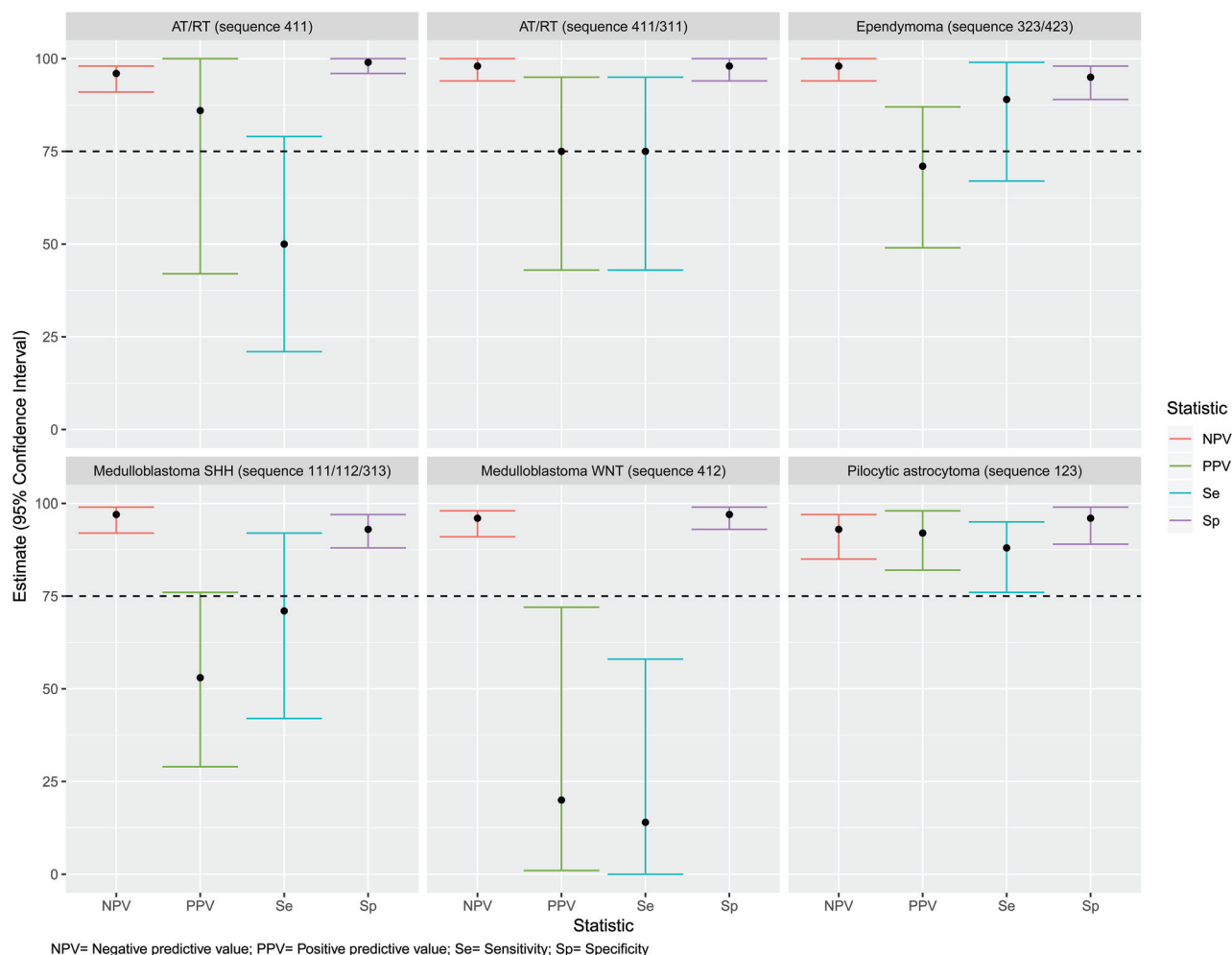
FIG 2. Diagnostic accuracy of a predesigned radiologic flow chart to identify different types of cerebellar tumors.

Table 1: Statistical analysis of the radiologic flow chart to discriminate different types of cerebellar tumors

Diagnosis Equivalent	Flowchart Sequence	Sensitivity (%)	Specificity (%)	PPV (%)	NPV (%)	Accuracy (%)
Ependymoma	323/423	89 (67–99)	95 (89–98)	71 (49–87)	98 (94–100)	94 (89–97)
Pilocytic astrocytoma	123	88 (76–95)	96 (89–99)	92 (82–98)	93 (85–97)	93 (87–96)
AT/RT	411	50 (21–79)	99 (96–100)	86 (42–100)	96 (91–98)	99 (96–100)
AT/RT	411/311	75 (43–95)	98 (94–100)	75 (43–95)	98 (94–100)	91 (96–98)
Medulloblastoma *SHH*	111/112/313	71 (42–92)	93 (88–97)	53 (29–76)	97 (92–99)	72 (64–79)
Medulloblastoma *WNT*	412	14 (0–58)	97 (93–99)	20 (1–72)	96 (91–98)	88 (93–97)

completely different cellular populations with different molecular profiles and different embryologic origins implies that they develop along different cellular paths. Thus, tumors that were previously considered as a single group can now be differentiated on imaging by location, age, and/or the patient's signal characteristics, resulting in a more accurate prognosis.[16-18]

In light of the crucial role of molecular profiling in tumor diagnosis and management, we found that the predesigned flow chart was very useful for categorizing and better understanding pediatric brain tumors. The importance of molecular profiling in the pediatric neuro-oncology clinical practice was first studied in medulloblastomas but is now recognized for ependymomas, low-grade astrocytomas, AT/RTs, and all previously classified primitive neuroectodermal tumors.[6,18-22]

Yet, since the 2016 classification update, several newly identified radiologic markers have been proposed as surrogates for the molecular diagnosis. The role of these radiologic markers may be limited by the constant evolution of the molecular characterization of brain tumors.[8,11] However, we believe that a standardized method of evaluating images, such as the proposed flow chart, may facilitate increased diagnostic accuracy.

The initial predesigned diagnostic flow chart has proved reliable and consistently accurate in this validation study, with an almost perfect agreement between 2 blinded neuroradiologists at 2 different institutions. Our results showed high coefficients of specificity and NPV for all diagnoses included in the predesigned flow chart. Sensitivity coefficients were high (>87%) for diagnosing pilocytic astrocytoma and ependymomas, the 2 most common diagnoses in
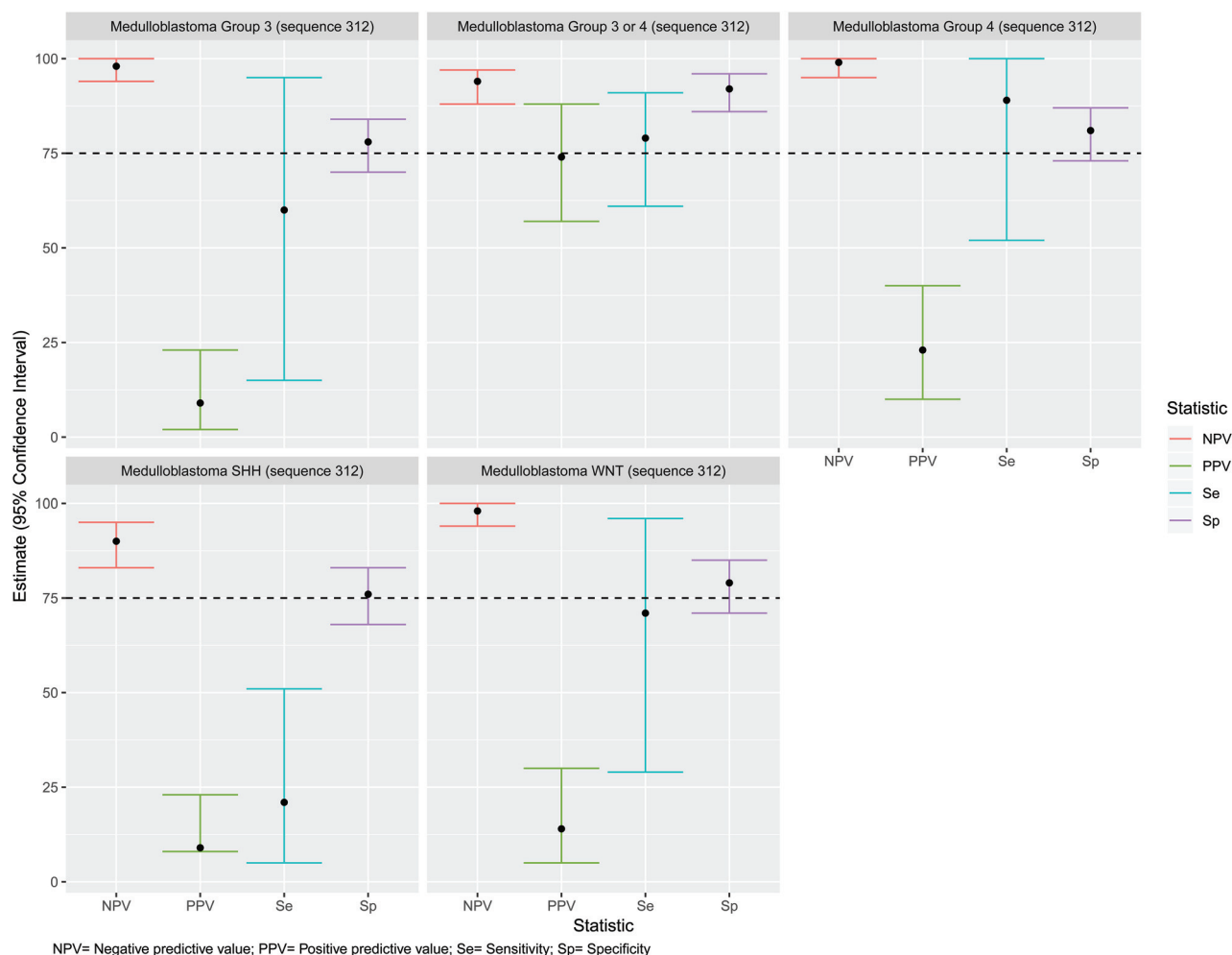
FIG 3. Diagnostic accuracy of sequence 312 (all types of medulloblastomas) of the predesigned radiologic flow chart to identify different types of medulloblastomas.

Table 2: Likelihood ratio analysis of the radiologic flow chart to discriminate different types of cerebellar tumors

Diagnosis	Flow Chart Sequence	LR+ (95% CI)	LR− (95% CI)
AT/RT	411/311	34 (10.6–109)[a]	0.26 (0.1–0.7)
Ependymoma	323/423	16.5 (7.9–35)	0.11 (0.03–0.4)[a]
Medulloblastoma *SHH*	111/112/313	10.6 (5.2–21.7)	0.3 (0.1–0.7)
Medulloblastoma group 3 or 4	312	10.07 (5.3–19.3)	0.23 (0.12–0.45)[a]
Pilocytic astrocytoma	123	20 (7.7–52.8)	0.13 (0.13–0.26)[a]

[a] Clinically applicable confidence intervals.

our cohort. Moreover, PA and ependymoma tumors had the smallest 95% CIs, suggesting reliability in the diagnosis of these 2 types of tumors. This was especially true for PA, in which the lower 95% CI limit for sensitivity was 76%, and for PPV, it was 82%.

After analyzing results from the initial flow chart created on the basis of more recently published literature, we modified it to improve diagnostic accuracy. Our modifications (see Figs 1 and 4 for comparison) successfully improved the sensitivity coefficient for identification of AT/RTs to 75%, but the confidence interval remained wide. The second modification to flow chart sequence 312 made possible the identification of most cases of medulloblastoma

group 3 or 4, with fair-to-good sensitivity (61%–91%) and PPV (57%–88%) and good-to-excellent specificity (86%–96%) and NPV (88%–97%). The modified flow chart (Fig 4) proved to be more clinically relevant. The modified flow chart proved capable of discriminating AT/RTs, ependymomas, medulloblastomas *SHH*, medulloblastoma groups 3 and 4, and PA, which together constitute 90.5% of tumors in our cohort. Clinically, the flow chart demonstrates great performance in ruling out group 3 or 4 medulloblastomas, PAs, and ependymomas and ruling in AT/RTs.

However, when it came to correctly identifying *WNT* medulloblastoma (numeric sequence 412, Fig 2), diagnostic accuracy was poor. In the predesigned flow chart, the authors designated a tumor in the pontocerebellar angle/foramen of Luschka with high cellularity (ie, low ADC) and patient age older than 3 years as suggestive of *WNT*. The rationale was that the cellular path of embryologic precursors, which can transform into neoplastic *WNT* cells, arises from the fourth ventricle down and laterally into the foramen of
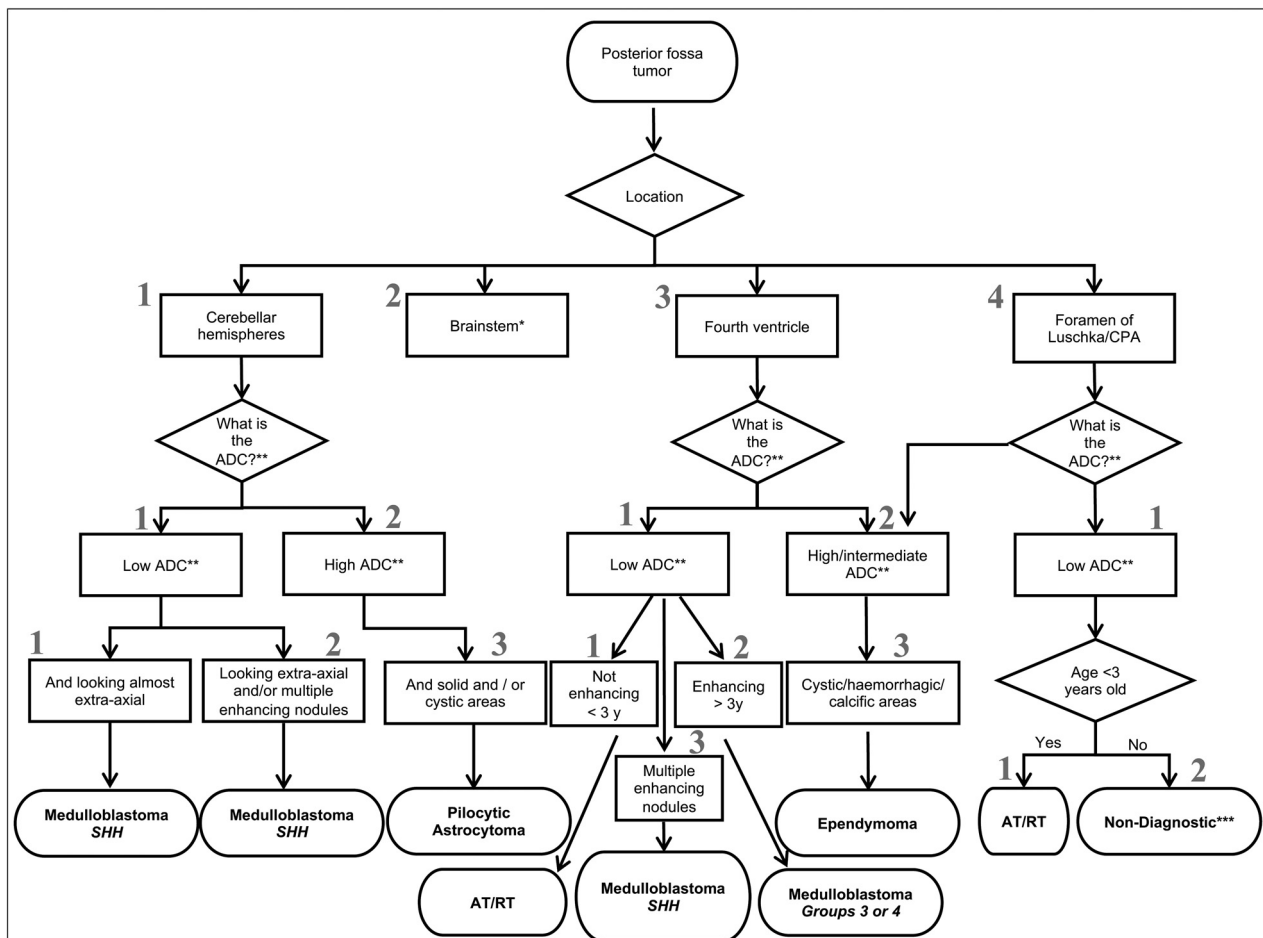
FIG 4. Modified radiologic flow chart (flow chart 2) after diagnostic accuracy analysis. The *asterisk* indicates brain stem tumors excluded from the analysis. *Double asterisks* indicate relative to gray matter. *Triple asterisks* indicates low PPV and sensitivity for any particular molecular/histological group of tumor.

Luschka.[7] The only other tumor with striking diffusion restriction in the Luschka area is AT/RT, but this is typical of younger children.[23] These results can be explained by several factors: the small number of *WNT* tumors present in our series (10% of all medulloblastomas), most cases in our series being in the fourth ventricle (which is understandable given that the path of the *WNT* cells is thought to start from the fourth ventricle), and the presence of anaplastic ependymomas showing diffusion restriction (therefore simulating *WNT* medulloblastoma on imaging).[24] More recently, a study of a larger cohort of *WNT* medulloblastomas has shown that they are not as lateralizing as previously reported in smaller cohorts.[25]

This study has some limitations, the main one being its retrospective nature. However, we controlled potential biases by doing a blinded review of images by only including cases with images obtained before surgical intervention and creating the baseline flow chart before data collection. Another important limitation is the relatively small number of cases for some types of tumor, which explains the larger confidence intervals for certain tumors. Nevertheless, many pediatric cerebellar tumors are relatively rare, and this is perhaps one of the largest cohorts available in the literature.[26] Moreover, we were able to gather a large enough cohort to allow diagnostic accuracy tests for the most common types of pediatric cerebellar tumors, with reliable results for most diagnoses.

Because this was planned as a validation study, we consider it successful in providing results that show that the modified flow chart can be used, is reliable, and has clinical applicability.

More research is still desired, with a larger consistency analysis evaluating results from multiple blinded readers. A larger prospective study would be needed to evaluate the diagnostic efficacy of the modified flow chart with higher precision. Such a study could provide an initial decision model for potential deep learning studies. Artificial intelligence is already being used to predict the molecular profile of brain tumors, most commonly in adult populations, but with recent important studies emerging in pediatric populations.[27,28] The main limitation for the application of machine learning in posterior fossa tumors may be the identification of tumor location,[29] because we know that signal characteristics (which reflect at least partially histologic appearances) can be similar for different molecular groups with similar tissue features. Currently, artificial intelligence is not able to differentiate tumors with the necessary level of precision, though this may be possible in the future.

CONCLUSIONS

A flow chart for the diagnosis of posterior fossa tumors in children has been validated through a retrospective analysis of 148 patients with confirmed diagnoses. On the basis of analysis of these
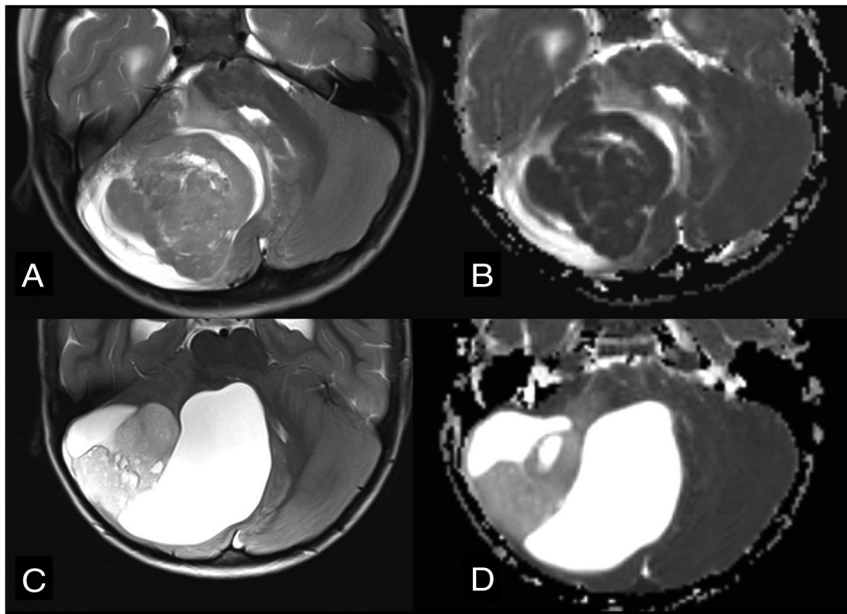
FIG 5. Differential diagnoses in cases of posterior fossa tumors originating from the cerebellar hemisphere. Axial T2WI (*A*) and axial ADC map (*B*) show *SHH* medulloblastoma (flow chart 2, number 111) in a typical peripheral location within the cerebellar hemisphere due to its origin from ganglionic cell precursors. Note very low ADC values (ie, diffusion restriction). Axial T2WI (*C*) and axial ADC map (*D*) show the typical appearance of a pilocytic astrocytoma (flow chart 2, number 123) originating from the cerebellar hemisphere. Note the typical nodule and appearance of cysts and much higher ADC values in comparison with the medulloblastoma.
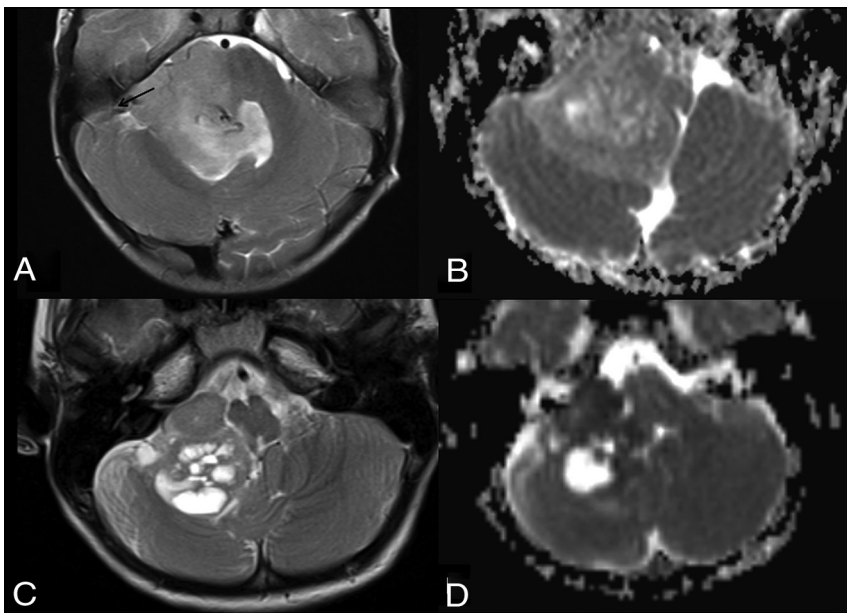
FIG 6. Differential diagnoses in posterior fossa tumors involving the foramen of Luschka and cerebellopontine angle. Axial T2WI (*A*) and ADC map (*B*) in a child with ependymoma (flow chart 2, number 423). Note the presence of internal vessels (*arrow*) and intermediate ADC values. Axial T2 (*C*) and ADC maps (*D*) in a 2-year-old boy with a AT/RT (new flow chart number 411). Note very low values of ADC, suggesting an embryonal tumor and peripheral cysts.

results, the predesigned flow chart was accurate in identifying most diagnoses, and with our subsequent modifications, the overall accuracy improved. The modified flow chart showed a good likelihood ratio for most of the histologic and molecular groups of tumors. Furthermore, it may offer an important starting point for prospective analysis using machine learning techniques. As new molecular subgroups emerge in the classification of pediatric brain tumors, there is the potential for further modifications to the flow chart to aid in diagnosis.

REFERENCES

1. Chhabda S, Carney O, D'Arco F, et al. **The 2016 World Health Organization Classification of Tumours of the Central Nervous System: what the paediatric neuroradiologist needs to know.** *Quant Imaging Med Surg* 2016;6:486–89 CrossRef Medline
2. Louis DN, Perry A, Reifenberger G, et al. **The 2016 World Health Organization Classification of Tumors of the Central Nervous System: a summary.** *Acta Neuropathol* 2016;131:803–20 CrossRef Medline

3. Taylor MD, Northcott PA, Korshunov A, et al. **Molecular subgroups of medulloblastoma: the current consensus.** *Acta Neuropathol* 2012;123:465–72 CrossRef Medline

4. Ramaswamy V, Remke M, Bouffet E, et al. **Risk stratification of childhood medulloblastoma in the molecular era: the current consensus.** *Acta Neuropathol* 2016;131:821–31 CrossRef Medline

5. Nowak J, Nemes K, Hohm A, et al. **Magnetic resonance imaging surrogates of molecular subgroups in atypical teratoid/rhabdoid tumor.** *Neuro Oncol* 2018;20:1672–79 CrossRef Medline

6. Pajtler KW, Witt H, Sill M, et al. **Molecular classification of ependymal tumors across all CNS compartments, histopathological grades, and age groups.** *Cancer Cell* 2015;27:728–43 CrossRef Medline

7. Patay Z, DeSain LA, Hwang SN, et al. **MR imaging characteristics of wingless-type-subgroup pediatric medulloblastoma.** *AJNR Am J Neuroradiol* 2015;36:2386–93 CrossRef Medline

8. Perreault S, Ramaswamy V, Achrol AS, et al. **MRI surrogates for molecular subgroups of medulloblastoma.** *AJNR Am J Neuroradiol* 2014;35:1263–69 CrossRef Medline

9. D'Arco F, Culleton S, De Cocker LJL, et al. **Current concepts in radiologic assessment of pediatric brain tumors during treatment, Part 1.** *Pediatr Radiol* 2018;48:1833–43 CrossRef Medline

10. Tamrazi B, Mankad K, Nelson M, et al. **Current concepts and challenges in the radiologic assessment of brain tumors in children, Part 2.** *Pediatr Radiol* 2018;48:1844–60 CrossRef Medline

11. D'Arco F, Khan F, Mankad K, et al. **Differential diagnosis of posterior fossa tumours in children: new insights.** *Pediatr Radiol* 2018;48:1955–63 CrossRef Medline

12. von Elm E, Altman DG, Egger M, et al. STROBE Initiative. **The Strengthening the Reporting of Observational Studies in Epidemiology (STROBE) statement: guidelines for reporting observational studies.** *Epidemiology* 2007;18:800–04 CrossRef Medline

13. McGee S. **Simplifying likelihood ratios.** *J Gen Intern Med* 2002;17:646–49 CrossRef Medline

14. Srinivasan VM, Ghali MG, North RY, et al. **Modern management of medulloblastoma: molecular classification, outcomes, and the role of surgery.** *Surg Neurol Int* 2016;7:S1135–41 CrossRef Medline

15. Kuzan-Fischer CM, Juraschka K, Taylor MD. **Medulloblastoma in the molecular era.** *J Korean Neurosurg Soc* 2018;61:292–301 CrossRef Medline

16. Raybaud C, Ramaswamy V, Taylor MD, et al. **Posterior fossa tumors in children: developmental anatomy and diagnostic imaging.** *Childs Nerv Syst* 2015;31:1661–76 CrossRef Medline

17. Poretti A, Meoded A, Huisman TA. **Neuroimaging of pediatric posterior fossa tumors including review of the literature.** *J Magn Reson Imaging* 2012;35:32–47 CrossRef Medline

18. Treisman DM, Li Y, Pierce BR, et al. **Sox2+ cells in sonic hedgehog-subtype medulloblastoma resist p53-mediated cell-cycle arrest response and drive therapy-induced recurrence.** *Neurooncol Adv* 2019;11:vdz027 CrossRef Medline

19. Wang J, Garancher A, Ramaswamy V, et al. **Medulloblastoma: from molecular subgroups to molecular targeted therapies.** *Annu Rev Neurosci* 2018;41:207–32 CrossRef Medline

20. Drezner NL, Packer RJ. **The impact of molecular analysis on the survival of children with embryonal tumors.** *Transl Pediatr* 2016;51:5–8 CrossRef Medline

21. Ho B, Johann PD, Grabovska Y, et al. **Molecular subgrouping of atypical teratoid/rhabdoid tumors (ATRT): a reinvestigation and current consensus.** *Neuro Oncol* 2020;22:613–24 CrossRef Medline

22. Venneti S. **Integrating ependymoma molecular subgroups into clinical trials.** *Neuro Oncol* 2019;21:1219–20 CrossRef Medline

23. Meyers SP, Khademian ZP, Biegel JA, et al. **Primary intracranial atypical teratoid/rhabdoid tumors of infancy and childhood: MRI features and patient outcomes.** *AJNR Am J Neuroradiol* 2006;27:962–71 Medline

24. Northcott PA, Dubuc AM, Pfister S, et al. **Molecular subgroups of medulloblastoma.** *Expert Rev Neurother* 2012;12:871–84 CrossRef Medline

25. Stock A, Mynarek M, Pietsch T, et al. **Imaging characteristics of wingless pathway subgroup medulloblastomas: results from the German HIT/SIOP-Trial cohort.** *AJNR Am J Neuroradiol* 2019;40:1811–17 CrossRef Medline

26. Hanzlik E, Woodrome SE, Abdel-Baki M, et al. **A systematic review of neuropsychological outcomes following posterior fossa tumor surgery in children.** *Childs Nerv Syst* 2015;31:1869–75 CrossRef Medline

27. Iv M, Zhou M, Shpanskaya K, et al. **MR imaging-based radiomic signatures of distinct molecular subgroups of medulloblastoma.** *AJNR Am J Neuroradiol* 2019;40:154–61 CrossRef Medline

28. Sotoudeh H, Shafaat O, Bernstock JD, et al. **Artificial intelligence in the management of glioma: era of personalized medicine.** *Front Oncol* 2019;9:768 CrossRef Medline

29. Tang TT, Zawaski JA, Francis KN, et al. **Image-based classification of tumor type and growth rate using machine learning: a preclinical study.** *Sci Rep* 2019;9:12529 CrossRef Medline